Royal Norwegian Council
for Scientific and Industrial Research
(NTNF)

NORSAR

NORSAR Scientific Report No. 1-90/91

Semiannual Technical Summary

1 April — 30 September 1990

Kjeller, November 1990

7.5 Real-time processing using a hybrid 3-component / small array station

Introduction

In recent years, much effort has been devoted to developing and assessing various methods for 3-component seismic data processing. It has been demonstrated that polarization analysis can provide P azimuth estimates with good accuracy from a single 3-component station. Using SH or SV particle motion models, some success has also been reported in determining azimuth from S and Lg phases, although there is often a 90 or 180 degree ambiguity in the resulting estimates.

These efforts notwithstanding, a fundamental problem in automatic 3-component processing still remains. This is the problem of phase identification, which of course is essential in deciding which particle motion model to apply. From our experience at NORESS, a high degree of rectilinearity, which in theory would indicate the presence of a P phase, is quite often seen also for S and Lg phases, and even for noise bursts, when applying polarization analysis. As a result, an automatic P-type solution found by 3-component processing is often of limited usefulness, since it may either be a P phase (with correct azimuth) or some other phase (in which case the azimuth estimate is useless).

Small-aperture arrays of the NORESS-type have proved to be very effective in processing regional as well as teleseismic phases. Their primary features are:

- Significant SNR gains at high frequencies
- Reliable phase identification (P-type versus S-type phases)
- Precise azimuth estimates of all phase types.

While the accuracy of NORESS azimuth estimates can be as good as $\pm$ 1 degrees for well-calibrated regions, the uncertainty of uncalibrated azimuth estimates is often of the order of 10 degrees or more, due to lateral inhomogeneities near the receivers. In practical schemes for automatic phase association (e.g., Mykkeltveit and Bungum, 1984), a tolerance of 30 degrees in azimuth deviation from the true value is often assumed. Given that the acceptable limits in azimuth estimation for phase association purposes are much less restrictive than the optimum array capability, a natural question is whether a smaller regional array can achieve reliable phase identification as well as an acceptable uncertainty in azimuth estimation.

We have attempted to address this question, and have chosen to evaluate the smallest such array available to us: the NORESS A-ring subarray (Fig. 7.5.1). This subarray comprises a center 3-component seismometer A0, surrounded by a triangular SPZ array A1–3. The diameter of this subarray is

only 0.3 km, i.e., a factor of 10 less than NORESS, and it thus spans an area only 1 per cent of that of the full NORESS array. In this paper, we present an initial evaluation of automatic detection processing using this very small array.

Automatic processing

We conducted automatic detection processing of the A-ring subarray for a period of 5 days (22–26 October 1990), using a standard multi-filter power detector with parameters as specified in Table 7.5.1. For each detected signal, broadband F-K analysis was conducted using the 4 SPZ sensors, and compared to the NORESS F-K results. We also carried out polarization analysis (using a P-wave particle motion model) for each detected phase, applying the method of Kværna and Doornbos (1986) to the 3-component A0 system.

To obtain a data base for the evaluation, we extracted all seismic phases detected by NORESS and associated to verified regional events for the 5-day period. The generalized beamforming procedure (Ringdal and Kværna, 1989) and the results from IMS processing (Bache *et al*, 1990) were used in order to ensure correct location of these reference events. P-coda detections and multiple S-phases were ignored, so that each event provided a maximum of 3 phases (P, S and Lg). These phases were then matched to the detection lists produced from the A-ring SPZ subarray and the 3-component analysis, and the phase velocity and azimuth estimates were compared.

Phase identification

Fig. 7.5.2 shows the A-ring phase velocity F-K estimates for P phases (circles) and S phases (crosses) for the reference data set. The separation is better than 95 per cent, which implies that even this small array is able to provide correct phase identification automatically and with high confidence. The corresponding picture for the full NORESS array is shown in Fig. 7.5.3, and naturally shows a better separation. It should be noted here that all the reference phases were by definition correctly identified by NORESS, so it is not surprising that the separation is 100 per cent. But it is still interesting to compare the scatter in the two data sets.

P-wave azimuths

Fig. 7.5.4 compares P-wave azimuths estimated by the full NORESS SPZ array and the small A-ring SPZ subarray using broadband F-K analysis in both cases. The estimates are very consistent, and the large majority are well within a tolerance limit of 30 degrees.

A corresponding plot for P waves analyzed from 3-component records is given in Fig. 7.5.5, and shows a similar amount of scatter. In fact, the scatter is slightly less than in Fig. 7.5.4. Thus, the polarization analysis can give very useful contributions to regional azimuth estimates, assuming that the

phase first has been identified as a P phase. An interesting approach would be to combine the two azimuth estimates (A-ring SPZ and 3-comp) in order to obtain increased stability.

S-wave azimuths

Fig. 7.5.6 compares azimuths of S-type phases estimated by the A-ring SPZ subarray and the full NORESS array. Again, the correspondence is quite good, and thus shows that automatic regional phase association using RONAPP-type processing can be achieved even when using an array as small as 0.3 km in diameter. We note that our 3-component processing provides no useful azimuth information for S phases, but it is of course possible that such information could be obtained in certain cases, given that the phase first has been identified as S or Lg.

Detectability

Figs. 7.5.7 and 7.5.8 illustrate the P and S wave detectability of the A-ring array as a function of NORESS SNR. From Fig. 7.5.7, it is seen that all P phases with SNR > 20 dB (i.e., STA/LTA > 10 at NORESS) have been detected. At distances below 500 km, several events of relatively low SNR at NORESS have also A-ring detections; this is due to the high signal frequencies which cause the full array SNR gains of these phases to be less than the theoretical $\sqrt{N}$. At distances above 500 km, the superiority of the full NORESS array becomes apparent.

In Fig. 7.5.8 it is seen that the A-ring subarray is close to matching NORESS S-phase detectability at all distances. This is because the horizontal components of the A0 3-component system provide quite efficient detection of S and Lg phases, in particular when added incoherently to the vertical component. The full array does not have the same SNR gain for secondary phases as for P-phases, because of less signal coherency and (in particular) coherent noise caused by P coda. Thus, as expected, there is not a significant difference in secondary phase detection.

False alarm consideration

In practical operation of any seismic system, the problem of false detections is very important. This is especially the case if the online detector is operated at a low detection threshold, and it is essential to be able to identify false alarms at as early a stage as possible.

To address this problem, we have analyzed in detail all the A-ring detections for one full data day (24 October 1990). The results are presented in Table 7.5.2, again with NORESS results as a reference. From the table, it is seen that out of 117 total phase detections, 105, or 90 per cent, were correctly classified using the broadband F-K analysis applied to A-ring SPZ data. Of these 105 phases, 37 were P, 36 S (or Lg) and 32 noise (i.e., low-velocity de-

tections). Note that P coda detections were counted as P and S coda were counted as S in these statistics. None of the 37 phases which (according to NORESS) were of the P type were misclassified by the A-ring. Of the 40 S phases, 4 were misclassified (2 P and 2 noise). Out of 40 noise detections, 3 were given P-phase velocities and 5 were given S-phase velocities when using the A-ring.

These statistics must be considered quite satisfactory. In fact, it appears that the SNR threshold for the A-ring detector could be lowered significantly, and still produce a reasonable false alarm rate.

Conclusions

The problems encountered when using a 3-component system in a real-time automatic processing environment appear to be effectively alleviated by supplementing the 3-C system with a very small (aperture 0.3 km) 3-element array. Based on the studies in this paper of the NORESS A-ring subarray, we conclude that:

- Phase identification (P or S) can be reliably achieved (better than 95 % success rate) using F-K analysis of the A-ring array data.
- Azimuth estimates, with accuracy generally to within 30 degrees can be obtained for both P and S phases using A-ring array processing, and (at least) for P-phases using 3-component polarization analysis of the A0 3-component station..
- Good regional P-phase detectability can be obtained from the A-ring array out to 500 km epicentral distance. At greater distances, P-wave detectability relative to that of NORESS deteriorates sharply.
- Detectability of S-phases using the A-ring array is excellent at all distances, and comes close to matching that of the full NORESS array.
- The A-ring array analysis makes it possible to isolate the majority of noise detections, thus giving an acceptable false alarm rate for online operation.

It would be an interesting experiment to supplement some existing 3-component stations with a triangular small array as described here, and conduct network detection and location experiments. Before doing so, it is of course important to verify that these results can be obtained in other geological and geographical environments, e.g., by analyzing similar data for other existing arrays (ARCESS, GERESS, FINESA).

A very small array of the A-ring type is especially suited for processing high signal frequencies. In fact, one might consider a dense sensor deployment within the A-ring aperture, as an experiment aimed at conducting array processing at frequencies of 20–40 Hz. This would of course require a higher sampling rate than the 40 Hz currently used at NORESS. Array processing at these frequencies would be of particular interest in the context of developing methods for monitoring cavity decoupled explosions, which might have significant signal energy in this frequency band.

T. Kværna
F. Ringdal

References

Bache, T.C., S.R. Bratt, J. Wang, R.M. Fung, C. Kobryn and J. Given (1990): The Intelligent Monitoring System, *Bull. Seism. Soc. Am.*, Special Issue, in print.

Kværna, T. and D.J. Doornbos (1986): An integrated approach to slowness analysis with arrays and three-component stations, *NORSAR Semiannual Technical Summary, 1 Oct 1985 - 31 Mar 1986*, NORSAR Sci. Rep. No. 2-85/86, Kjeller, Norway.

Mykkeltveit, S. and H. Bungum (1984): Processing of regional seismic events using data from small aperture arrays, *Bull. Seism. Soc. Am.*, 74, 2313–2333.

Ringdal, F. and T. Kværna (1989): A multichannel processing approach to real time network detection, phase association and threshold monitoring, *Bull. Seism. Soc. Am.*, 79, 1927–1940.

Coherent beams:

Beam	Apparent vel.	Azimut	Filter band	Configuration	Threshold
NZ01	9999.9	0.0	0.5- 1.5	A0z,A1z,A2z,A3z	4.0
NZ02	9999.9	0.0	1.0- 2.0	A0z,A1z,A2z,A3z	3.7
NZ03	9999.9	0.0	1.0- 3.0	A0z,A1z,A2z,A3z	3.7
NZ04	9999.9	0.0	1.5- 2.5	A0z,A1z,A2z,A3z	3.5
NZ05	9999.9	0.0	1.5- 3.5	A0z,A1z,A2z,A3z	3.5
NZ06	9999.9	0.0	2.0- 3.0	A0z,A1z,A2z,A3z	3.5
NZ07	9999.9	0.0	2.0- 4.0	A0z,A1z,A2z,A3z	3.5
NZ08	9999.9	0.0	2.5- 4.5	A0z,A1z,A2z,A3z	3.5
NZ09	9999.9	0.0	3.0- 5.0	A0z,A1z,A2z,A3z	3.5
NZ10	9999.9	0.0	3.5- 5.5	A0z,A1z,A2z,A3z	3.7
NZ11	9999.9	0.0	4.0- 8.0	A0z,A1z,A2z,A3z	3.7
NZ12	9999.9	0.0	5.0-10.0	A0z,A1z,A2z,A3z	3.7
NZ13	9999.9	0.0	8.0-16.0	A0z,A1z,A2z,A3z	4.0

Incoherent beams:

Beam	Apparent vel.	Azimut	Filter band	Configuration	Threshold
NA01	9999.9	0.0	0.5- 1.5	A0z,A0n,A0e	2.7
NA02	9999.9	0.0	1.0- 2.0	A0z,A0n,A0e	2.6
NA03	9999.9	0.0	1.0- 3.0	A0z,A0n,A0e	2.5
NA04	9999.9	0.0	1.5- 2.5	A0z,A0n,A0e	2.5
NA05	9999.9	0.0	1.5- 3.5	A0z,A0n,A0e	2.5
NA06	9999.9	0.0	2.0- 3.0	A0z,A0n,A0e	2.6
NA07	9999.9	0.0	2.0- 4.0	A0z,A0n,A0e	2.8
NA08	9999.9	0.0	2.5- 4.5	A0z,A0n,A0e	3.4
NA09	9999.9	0.0	3.0- 5.0	A0z,A0n,A0e	3.5
NA10	9999.9	0.0	3.5- 5.5	A0z,A0n,A0e	2.8
NA11	9999.9	0.0	4.0- 8.0	A0z,A0n,A0e	2.5
NA12	9999.9	0.0	5.0-10.0	A0z,A0n,A0e	2.5
NA13	9999.9	0.0	8.0-16.0	A0z,A0n,A0e	2.8

Table 7.5.1. Parameters used for the A-ring detector experiment.

	Classified as:		
Correct Phase id	P (v>6 km/s)	S or Lg (3.4<v≤6 km/s)	Noise (v≤3.4 km/s)
P	37	0	0
S or Lg	2	36	2
Noise	3	5	32

Total phases detected by the A-ring detector : 117
Total phases correctly classified : 105 (90 %)

Table 7.5.2. Statistics of detected phases for the A-ring array for a 24-hour period. The phases are classified based on estimated phase velocities using A-ring SPZ broadband F-K, and the "correct" phase id is based on F-K results from the full NORESS array.

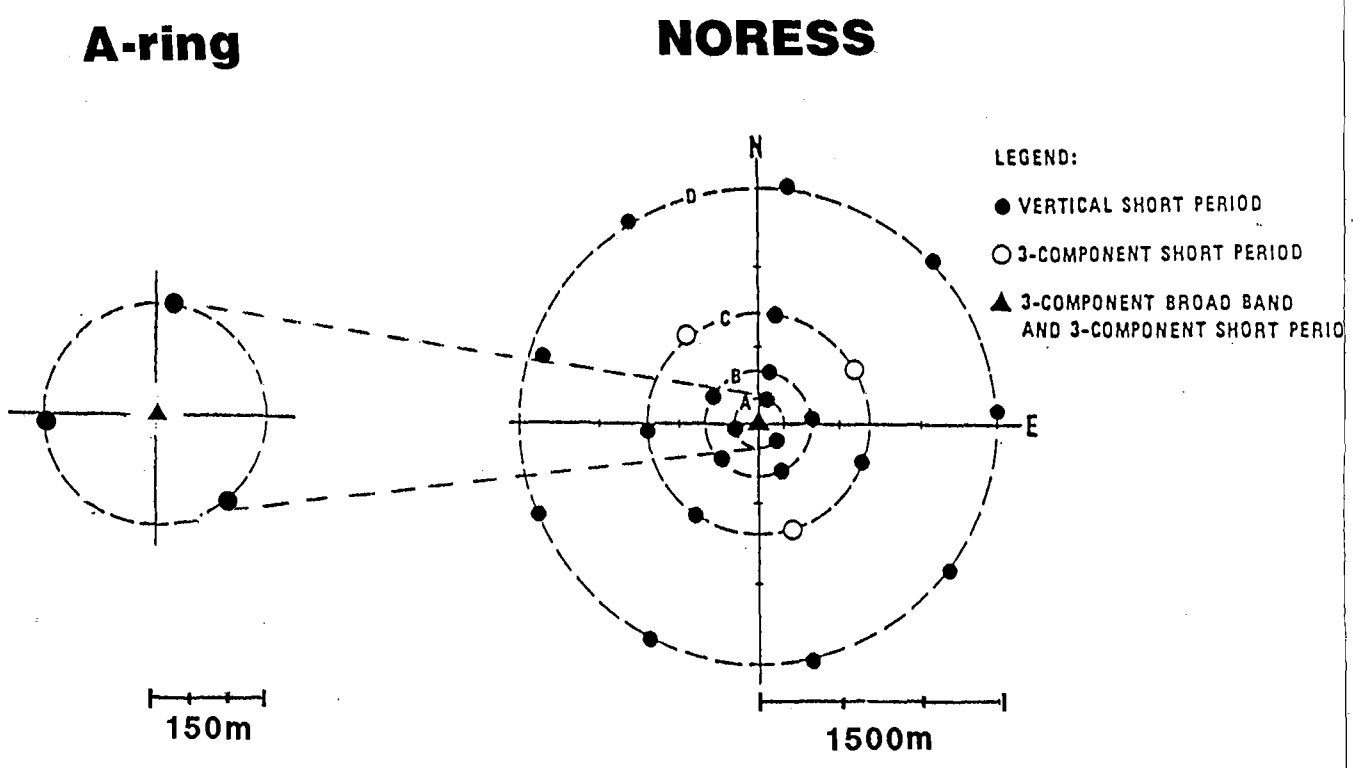

Fig. 7.5.1. Geometry of the full NORESS array and of the A-ring subarray used in this study.

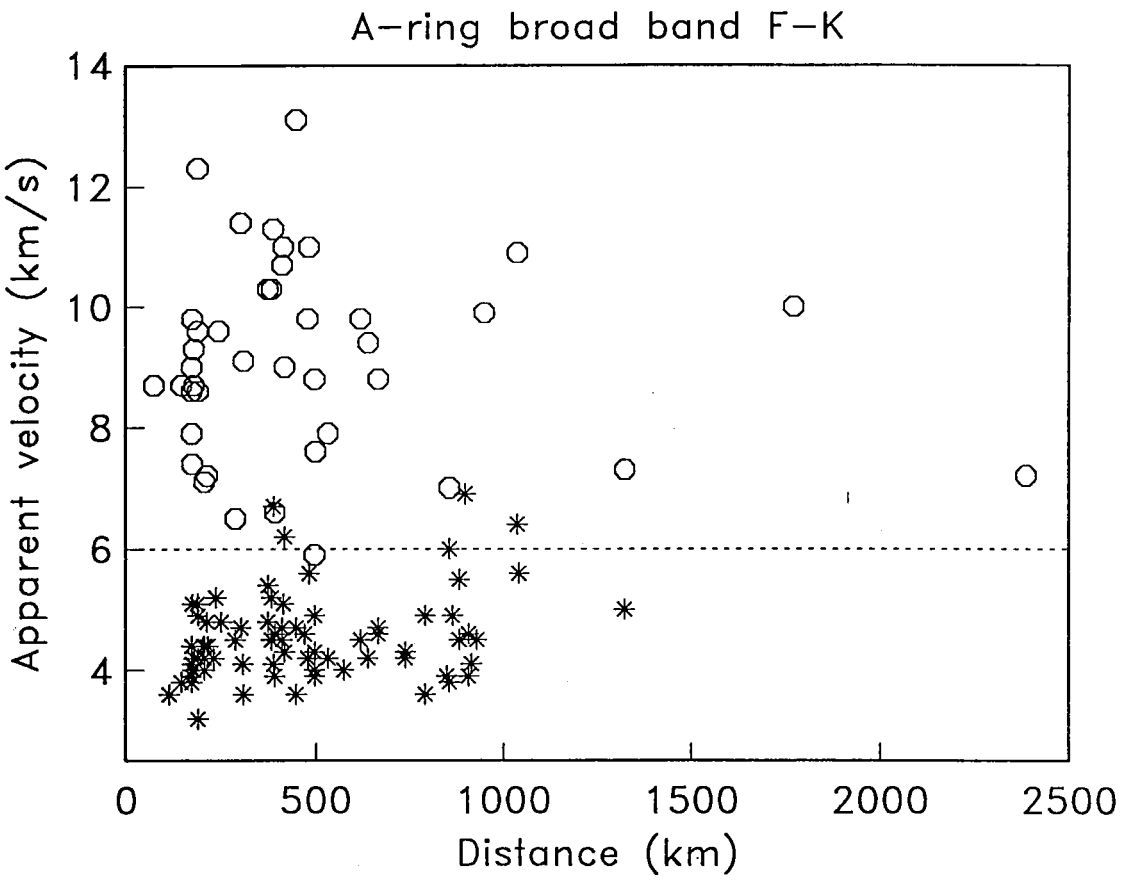

Fig. 7.5.2. Estimated phase velocities using the A-ring SPZ array (broadband F-K) for detected P phases (circles) and S phases (asterisks). Note that the phases can be identified from phase velocity with more than 95 % accuracy.

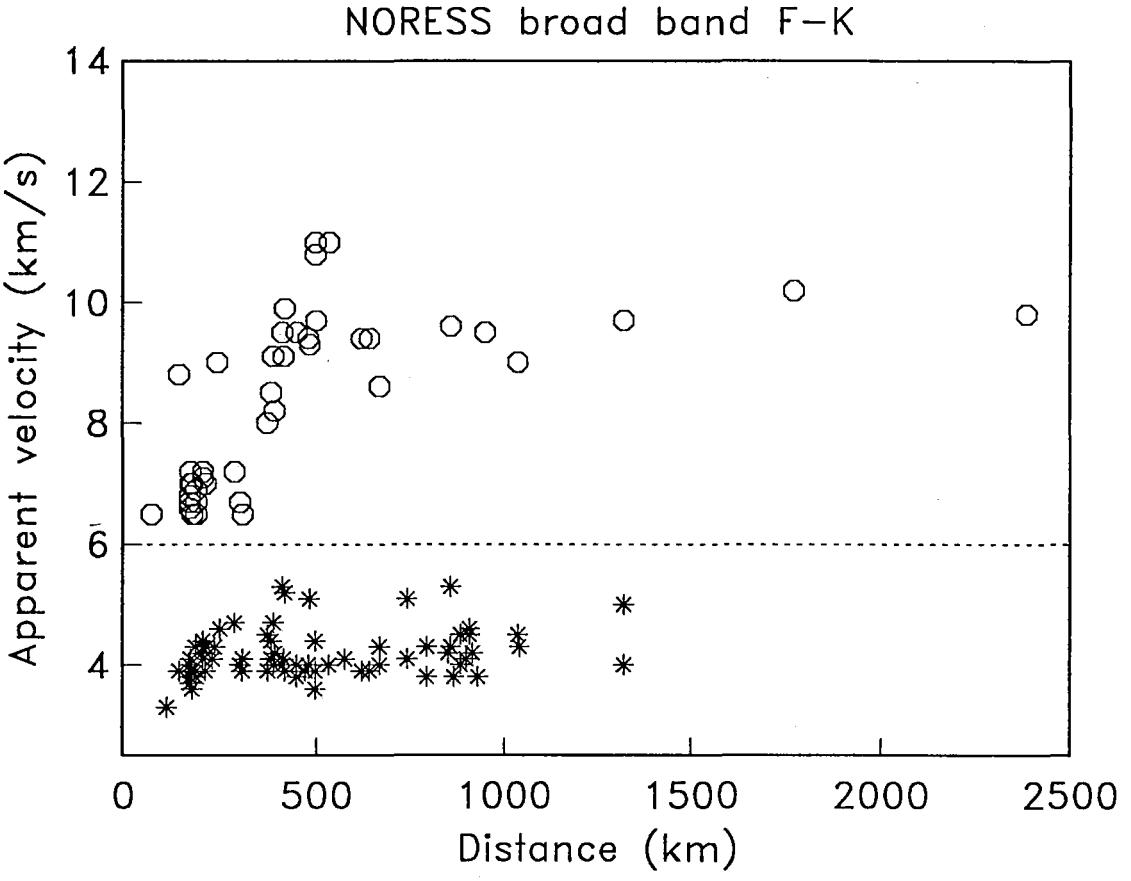

Fig. 7.5.3. Similar to Fig. 7.5.2, but with phase velocities estimated using the full NORESS array.

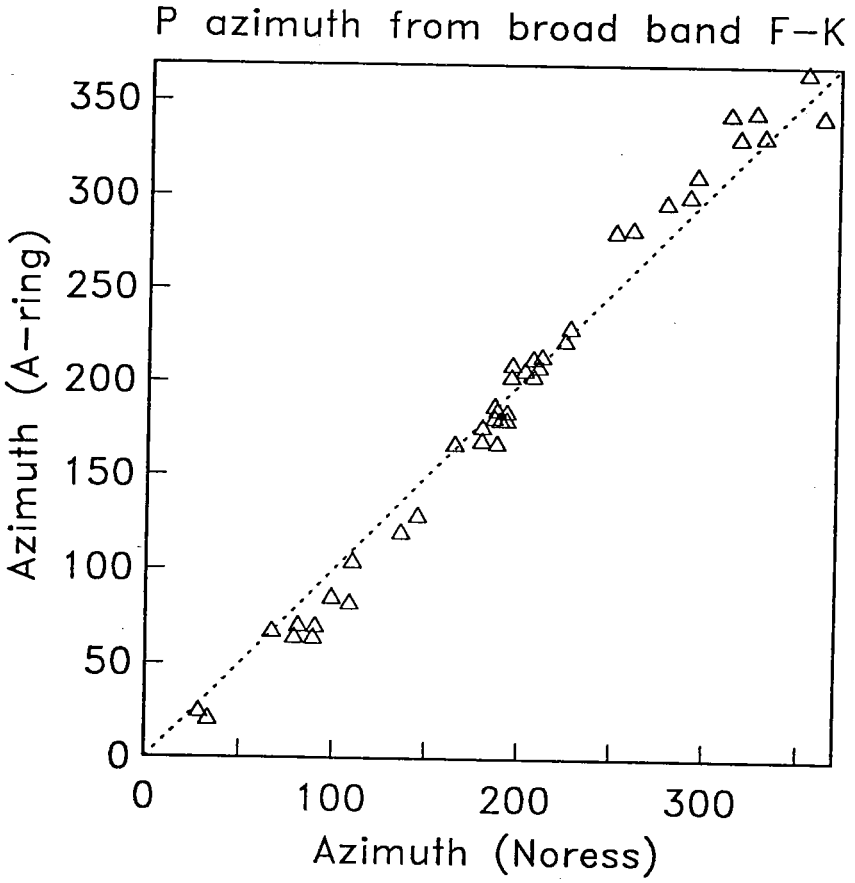

Fig. 7.5.4. Comparison of estimated azimuths of P phases using the full NORESS array and the A-ring SPZ array (broadband F-K). Note the excellent consistency.

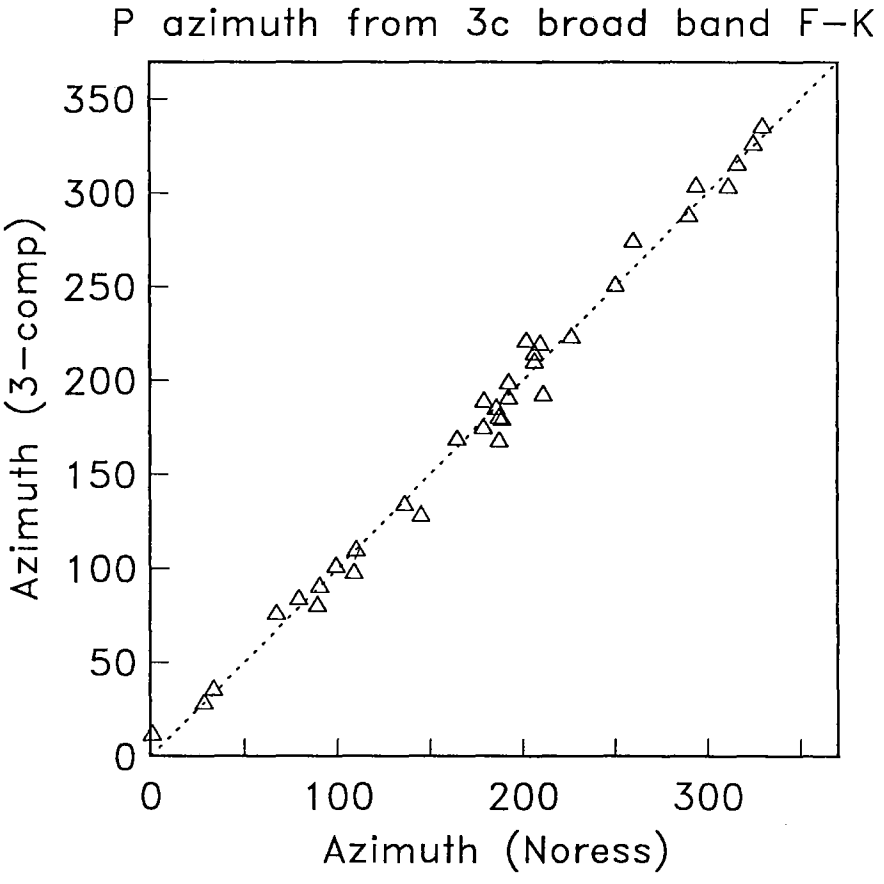

Fig. 7.5.5. Comparison of estimated azimuths of P phases using the full NORESS array (broadband F-K) and the A0 3-component system (polarization analysis). Note that the consistency is similar to that of Fig. 7.5.4.

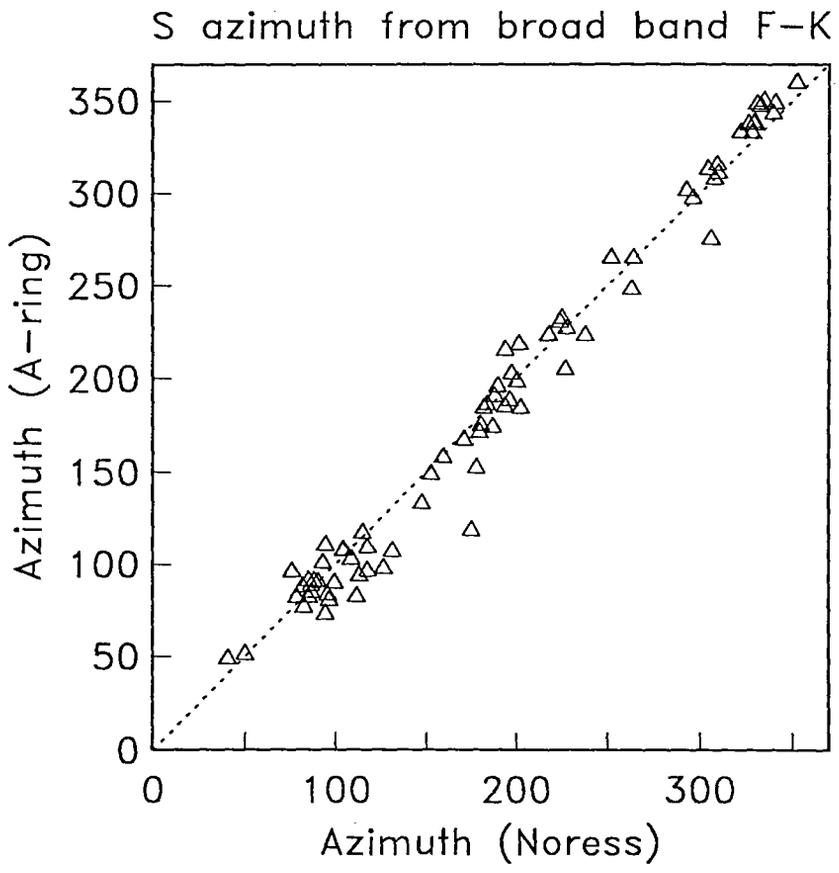

Fig. 7.5.6. NORESS and A-ring azimuth comparison for S phases. Note that the consistency is as good as for P phases (in Fig. 7.5.4).

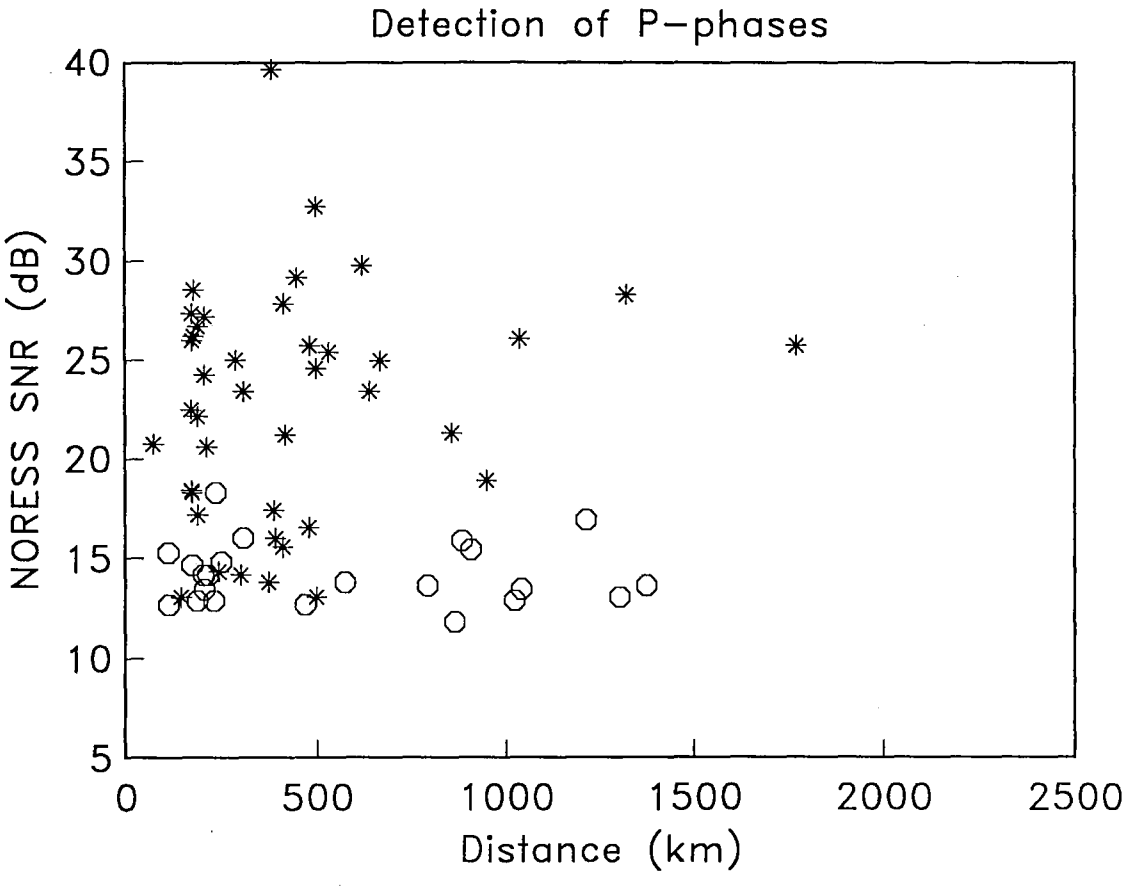

Fig. 7.5.7. Illustration of P-phase detectability of the A-ring SPZ array combined with the 3-component A0 system. P-phases detected by the A-ring SPZ/3-component system are marked as asterisks, whereas nondetected phases are marked as circles. Note that the reference array (NORESS) is clearly superior at distances > 500 km.

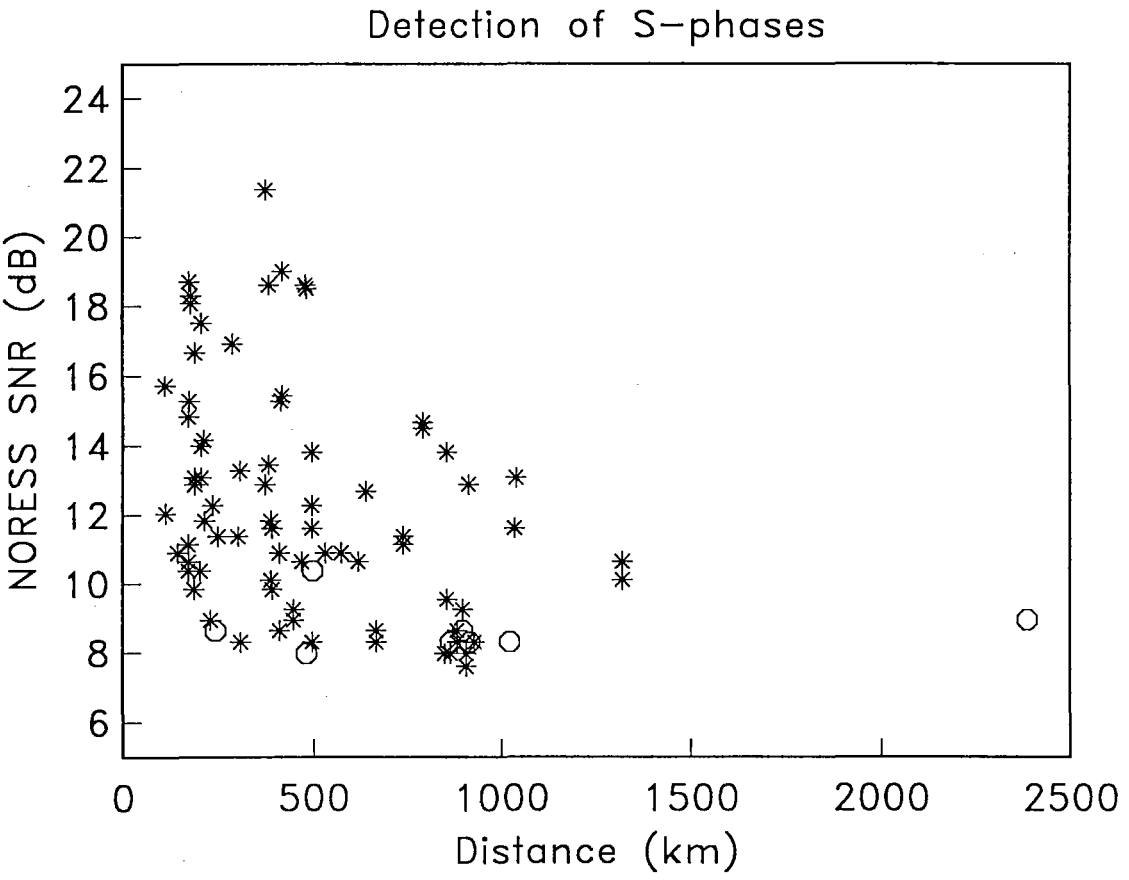

Fig. 7.5.8. Same as Fig. 7.5.7, but for S phases. Note that in this case the small array/3-component system comes close to matching the full array performance.